ACS Catalysis

Subscriber access provided by UNIV AUTONOMA DE COAHUILA UADEC

Article

In vitro and *in vivo* One-pot Deracemization of Chiral Amines by Reaction Pathway Control of Enantiocomplementary #-Transaminases

Sang-Woo Han, YOUNGHO JANG, and Jong-Shik Shin

ACS Catal., **Just Accepted Manuscript** • DOI: 10.1021/acscatal.9b01546 • Publication Date (Web): 09 May 2019

Downloaded from http://pubs.acs.org on May 10, 2019

Just Accepted

"Just Accepted" manuscripts have been peer-reviewed and accepted for publication. They are posted online prior to technical editing, formatting for publication and author proofing. The American Chemical Society provides "Just Accepted" as a service to the research community to expedite the dissemination of scientific material as soon as possible after acceptance. "Just Accepted" manuscripts appear in full in PDF format accompanied by an HTML abstract. "Just Accepted" manuscripts have been fully peer reviewed, but should not be considered the official version of record. They are citable by the Digital Object Identifier (DOI®). "Just Accepted" is an optional service offered to authors. Therefore, the "Just Accepted" Web site may not include all articles that will be published in the journal. After a manuscript is technically edited and formatted, it will be removed from the "Just Accepted" Web site and published as an ASAP article. Note that technical editing may introduce minor changes to the manuscript text and/or graphics which could affect content, and all legal disclaimers and ethical guidelines that apply to the journal pertain. ACS cannot be held responsible for errors or consequences arising from the use of information contained in these "Just Accepted" manuscripts.

ACS Publications

is published by the American Chemical Society. 1155 Sixteenth Street N.W., Washington, DC 20036

Published by American Chemical Society. Copyright © American Chemical Society. However, no copyright claim is made to original U.S. Government works, or works produced by employees of any Commonwealth realm Crown government in the course of their duties.

In vitro and *in vivo* One-pot Deracemization of Chiral Amines by Reaction Pathway Control of Enantiocomplementary ω-Transaminases

Sang-Woo Han,[†] *Youngho Jang*[†] *and Jong-Shik Shin**[,†]

[†] Department of Biotechnology, Yonsei University, Yonsei-Ro 50, Seodaemun-Gu, Seoul 03722, South Korea

ABSTRACT

Biocatalytic cascade conversion of racemic amines into optically pure ones using enantiocomplementary ω-transaminases (ω-TAs) has been developed by thermodynamic and kinetic control of reaction pathways where twelve competing reactions occur with pyruvate and isopropylamine used as cosubstrates. Thermodynamic control was achieved under reduced pressure for selective removal of a coproduct (i.e. acetone), leading to elimination of six undesirable reactions. Engineered orthogonality in substrate specificities of ω-TAs was exploited for kinetic control, enabling suppression of four additional reactions. Taken together, the net reaction pathway could be directed to two desired reactions, i.e. oxidative deamination of *R*-amine and reductive amination of the resulting ketone into antipode *S*-amine. This strategy afforded one-pot deracemization of various chiral amines with > 99 % ee_S and 85 - 99 % reaction yields of the resulting *S*-amine products. The *in vitro* cascade reaction could be successfully implemented in a live microbe using glucose or L-threonine as a cheap amino acceptor precursor, demonstrating a synthetic metabolic pathway enabling deracemization of chiral amines which has never been observed in living organisms.

KEYWORDS: deracemization, chiral amine, transaminase, protein engineering, metabolic engineering

INTRODUCTION

In vivo biochemical networks consist of a vast number of cascade reactions where reaction intermediates are processed by specific enzymes dedicated for each reaction step.[1-2] Coordination of the complex reaction pathways into a well-defined hierarchy is elegantly achieved by an exquisite combination of thermodynamic and kinetic control that keep the reaction fluxes under precise regulation.[3-4] Thermodynamically unfavorable reactions are coupled with energetic drivers such as ATP hydrolysis and NADH oxidation, so energy-consuming pathways are driven forward.[5] Undesirable exergonic reactions are kinetically suppressed by exploiting orthogonal substrate specificities of relevant enzymes with a minimal overlap that allows promiscuous utilization of common intermediates.[6] Construction of a synthetic metabolic pathway by mimicking the biological design principles is promising for coming up with novel bioprocesses that living organisms have not yet pursued.[7-10]

Although racemization is a naturally occurring reaction in living organisms to supply a minor enantiomer from a major antipode reservoir,[11-12] deracemization has never been observed in native metabolism presumably owing to the lack of biological demand for this functionality. However, deracemization is conceptually and commercially interesting in the chemical industry because preparation of racemic mixtures is usually readily available relying on conventional organic synthesis.[13] In the case of chiral amines that are essential building blocks of a number of pharmaceutical drugs,[14] deracemization remains a huge challenge for chemocatalytic approaches and instead employs biocatalytic methods which mostly rely on monoamine oxidase.[15-18] In the monoamine oxidase-based deracemization, racemic amines are stereoselectively oxidized by monoamine oxidase to imines which are reduced back to the amines without stereoselectivity by ammonia borane,[13, 15, 18] palladium formate/hydrogen[16] or artificial metalloenzyme.[17] It is notable

that complete deracemization requires oxidation of actually two equivalents of an unwanted enantiomer owing to the non-stereoselective reduction of the resulting imine. Recently, stereoselective reduction of the imine intermediate has been demonstrated using imine reductase for deracemization of 2-substituted piperidines and pyrrolidines.[19] More recently, Aleku et al. reported a new deracemization approach where monoamine oxidase was substituted by reductive aminase.[20]

Besides the monoamine oxidase-based approaches, deracemization of chiral amines was demonstrated using two enantiocomplementary ω-transaminases (ω-TAs) in a stepwise fashion, i.e. serial processing of the two ω-TA reactions in the presence of auxiliary enzymes for equilibrium shift.[21-23] More recently, native orthogonality in substrate specificity afforded one-pot deracemization where both ω-TA reactions occurred simultaneously.[24] This method was contingent on a non-canonical activity of an ω-TA from *Polaromonas* sp. for α-ketoglutarate. Note that ω-TAs known to date adopt pyruvate as a universal amino acceptor.[25-26] Therefore, applicability of this approach is limited because the enzyme from *Polaromonas* sp. is the only ω-TA, known to date, to be active for α-ketoglutarate.[24] Moreover, both cosubstrates (i.e., α-ketoglutarate and D-alanine) are expensive and additional enzymes should be supplied to overcome unfavorable equilibrium in the transamination between ketone and D-alanine. Setting up orthogonal substrate specificities of the two enzymes has been also demonstrated by coupling ω-TA and enantiocomplementary amine dehydrogenase.[27] However, to allow industrial feasibility, one should come up with a generally applicable strategy that employs cheap cosubstrates and facile equilibrium shift without relying on auxiliary enzymes and external cofactors.

In this study, we aimed at developing such a ω-TA-based protocol for deracemization of various chiral amines (**1a-f**) using typical cosubstrates such as pyruvate (**3**) and isopropylamine (**5**)

(Scheme 1). Note that **5** is one of the preferred amino donors for amination of ketones owing to a low price and easy removal of its deamination product, i.e. acetone (**6**), under reduced pressure.[28-29] As a proof-of-concept, we explored conversion of racemic amines into *S*-enantiomers via stereoinversion of unwanted *R*-enantiomers using a *R*-selective ω-TA from *Arthrobacter* sp. (ARTA)[30] and a *S*-selective one from *Ochrobactrum anthropi* (OATA).[31] Because **3** and **5** are common substrates for both ARTA and OATA, a number of competing reactions would occur in the reaction mixture charged with racemic amine, **3** and **5** in the presence of the two ω-TAs. Suppression of unwanted reactions was carried out using process and protein engineering strategies, leading to reaction pathway control that enabled the competing reactions to be directed to the two desired reactions consisting of an energetically down-hill amino group transfer between *R*-**1a**-**f** and **3** and an up-hill one between **2a**-**f** and **5**. We demonstrated that the reaction pathway control by combining thermodynamic and kinetic control afforded deracemization of chiral amines both *in vitro* and *in vivo*.

EXPERIMENTAL SECTION

Materials

S-**1e**, *R*-**1e**, *S*-**1f** and *R*-**1f** were purchased from Alfa Aesar (Ward Hill, MA, USA). **5** and L-threonine were obtained from Junsei Chemical Co. (Tokyo, Japan). Dimethyl sulfoxide (DMSO), methanol, ethanol, acetonitrile, glucose and sodium acetate were obtained from Duksan Pure Chemicals Co. (Ansan, South Korea). DL-**4** was purchased from Samchun Pure Chemical Co. (Seoul, South Korea). All other chemicals including racemic amines were purchased from Sigma-Aldrich Co. (St. Louis, MO, USA). Materials used for preparation of culture media were obtained from Difco (Spark, MD, USA).

Site-directed Mutagenesis of OATA

Construction of OATA carrying W58L and R417A substitutions ($OATA_{W58L/R417A}$) was performed using a QuikChange Lightning site-directed mutagenesis kit (Agilent Technologies Co.) according to an instruction manual. Mutagenesis PCR was performed using pET28-$OATA_{W58L}$, created previously,[32] as a template. Forward (5′-CGCGG CGTCATTTCCGCGGCA ATGGGCGATACG-3′) and reverse (5′-CGTATCGCCCATTGCCGCGGAAATGACG CCGCG-3′) primers for the mutagenesis were designed by a primer design program (https://www.genomics.agilent.com/ primerDesignProgram.jsp). The site-directed mutagenesis was verified by DNA sequencing.

Preparation of Purified ω-TAs

Expression and purification of His_6-tagged ω-TAs were performed as described before with minor modifications.[33] Expression vectors used for the protein expression were listed in Table S1. *Escherichia coli* BL21(DE3) cells were transformed with a pET28a(+) expression vector harboring a ω-TA gene and the transformant cells were cultivated in 1 L of LB medium containing 50 μg/mL kanamycin at 37 °C. Protein expression was induced by adding IPTG (final concentration = 0.1 mM) at $OD_{600} \approx 0.4$. After further cultivation at 37 °C for 12 h, cells were spun down by centrifugation (10,000×g, 10 min, 4 °C) and the resulting cell pellet was resuspended in 15 mL buffer (50 mM sodium chloride, 1 mM EDTA, 1 mM β-mercaptoethanol, 0.1 mM PMSF and 50 mM Tris, pH 8). Cells were disrupted by a sonicator, followed by centrifugation (10,000×g, 60 min, 4 °C) to remove cell debris. The resulting supernatant was used as cell-free extract for protein purification.

The cell-free extract was subjected to protein purification using a HisTrap HP column (GE Healthcare) on an ÄKTAprime plus (GE Healthcare). The His_6-tagged ω-TA was eluted by a linear gradient of imidazole (0.05-0.5 M imidazole, 0.15 M sodium chloride, 0.5 mM PLP and 20 mM sodium phosphate, pH 7.4). Desalting was carried out on a HiTrap HP column (GE Healthcare) using a buffer (0.15 M sodium chloride, 0.5 mM PLP and 50 mM sodium phosphate, pH 7). When necessary, the enzyme solution was concentrated by an Amicon Ultra-15 30K (Millipore Co.). Concentration of the purified ω-TA was determined by measuring UV absorbance at 280 nm with a UV-1650PC spectrophotometer (Shimadzu Co.). Molar extinction coefficients of the homodimeric ω-TAs were obtained by a protein extinction coefficient calculator (http://www.biomol.net/en/tools/proteinextinction.htm) and are listed in Table S1.

Enzyme Activity Assay

All the enzyme assays were carried out at 37 °C and pH 7 (50 mM potassium phosphate buffer). Initial reaction rates of ω-TAs for reactions using **1a**/**3**, **5**/**2a** and **5**/**3** as substrate pairs were measured at < 20 % conversion by HPLC analyses of **2a**, **1a** and **4**, respectively. Typical reaction volume was 100 μL and the reactions were stopped by adding 600 μL of acetonitrile, 37.5 μL of 16 % (v/v) $HClO_4$ and 20 μL of 5 N HCl for reactions using **1a**/**3**, **5**/**2a** and **5**/**3** as substrate pairs, respectively.

Determination of Rate Constants for Mathematical Modeling

To enable mathematical modeling with a minimum set of kinetic parameters, we assumed that the enzyme kinetics might be approximated to a second-order rate equation, i.e. first order with respect to each substrate concentration, by ignoring variation in the distribution of enzyme species such

as E-PLP, E-PMP and Michaelis complexes. Based on the pseudo-second-order approximation, reaction velocity (v_t) with respect to reaction time can be expressed by a following equation

$$v_t = k_{app}[\mathrm{A}]_t[\mathrm{D}]_t \quad \text{(Eq. 1)}$$

where k_{app} represents an apparent rate constant at a given enzyme concentration ([E]). $[\mathrm{A}]_t$ and $[\mathrm{D}]_t$ represent time-dependent concentrations of an amino acceptor (A) and a donor (D), respectively. Using Eq. 1, specific reaction rate (i.e., initial velocity per enzyme concentration; $v_i/[\mathrm{E}]$) can be expressed as follows.

$$v_i/[\mathrm{E}] = (k_{app}/[\mathrm{E}])[\mathrm{A}]_i[\mathrm{D}]_i \quad \text{(Eq. 2)}$$

Therefore, $k_{app}/[\mathrm{E}]$ values for ARTA, OATA and $\mathrm{OATA_{W58L/R417A}}$ could be obtained by dividing specific reaction rate with $[\mathrm{A}]_i$ and $[\mathrm{D}]_i$. Table S2 lists the $k_{app}/[\mathrm{E}]$ values. In the case of $\mathrm{OATA_{W58L}}$ and $\mathrm{OATA_{R417A}}$, the $k_{app}/[\mathrm{E}]$ values were taken from those of OATA and $\mathrm{OATA_{W58L/R417A}}$ by assuming that the activity changes by each point mutation are completely independent. Thus, it was assumed that the W58L substitution did not affect the reactions for **1a**/**3** and **5**/**3** substrate pairs but affected the reaction for **5**/**2a**. In contrast, the R417A substitution was assumed to affect the reactions for **1a**/**3**, and **5**/**3** substrate pairs but not the one for **5**/**2a**. The $k_{app}/[\mathrm{E}]$ values assigned for $\mathrm{OATA_{W58L}}$ and $\mathrm{OATA_{R417A}}$ are listed in Table S3. Numerical solutions of simultaneous differential equations for the competing reactions were obtained using the $k_{app}/[\mathrm{E}]$ values by the software Mathematica (Wolfram Research Inc.).

Small-scale Deracemization of Chiral Amines

All the deracemization reactions were performed at 37 °C and 460 Torr. The reduced pressure was achieved by a vacuum pump with a vacuum controller (EYELA Co.). Typical reaction volume was 1 mL and the reaction conditions were 10 mM *rac*-**1a**-**f**, 6.5 mM **3**, 100 mM **5**, 10 μM ARTA,

100 μM $OATA_{W58L/R417A}$ in 50 mM potassium phosphate buffer (pH 7) containing 15 % (v/v) DMSO. At the predetermined reaction time, aliquots of the reaction mixture (typical 50 μL) were taken and mixed with 18.75 μL of 16 % (v/v) $HClO_4$ to stop the reaction. Amines were analyzed by quantitative chiral HPLC, which were used for determination of reaction yield and enantiomeric excess. When the reaction yield exceeded 90 %, **3** was added in the reaction mixture for chiral polishing, and then running for 30 min (final concentration of **3** = 0.5 mM except 0.3 mM for *rac*-**1d**).

*Preparative-scale Deracemization and Product Characterization of S-**1d***

Preparative-scale deracemization of *rac*-**1d** was carried out at 37 °C and 460 Torr in 100 mL reaction mixture containing *rac*-**1d** (1.49 g, 10 mmol), **3** (0.88 g, 8 mmol), **5** (1.18 g, 20 mmol), ARTA (10 μM), $OATA_{W58L/R417A}$ (200 μM), 15 % (v/v) DMSO and 50 mM Tris buffer (pH 7). When the reaction yield exceeded 80 %, **3** was additionally added to the reaction mixture for chiral polishing (final concentration = 1.5 mM) and the reaction was allowed to proceed for 1.5 h.

Product isolation was carried out using ion-exchange chromatography. For protein removal, pH of the reaction mixture was adjusted to 1 by adding 5 N HCl and the resulting solution was centrifuged (10,000×g, 30 min), followed by filtration through a glass-fritted filter funnel. The filtrate solution was loaded on a glass column packed with Dowex 50WX8 cation-exchange resin (40 g). Washing and elution were carried out by sequentially loading water (40 mL) and 10 % (v/v) ammonia solution (800 mL). The eluates were collected and then *S*-**1d** was extracted three times with *n*-hexane (3×300 mL). The resulting extractant pool was evaporated at 50 °C and 0.45 bar, resulting in clear liquid of *S*-**1d**.

The isolated *S*-**1d** was structurally characterized by ^{1}H NMR, ^{13}C NMR and LC/MS. ^{1}H NMR and ^{13}C NMR spectra were recorded on an Avance II FT-NMR spectrometer (Bruker Co.) using tetramethylsilane as a standard. Mass spectral data were obtained with a LTQ Orbitrap Mass Spectrometer (electrospray ionization, positive ion mode, Thermo Fisher Scientific Inc.).

Construction of Expression Plasmids for in vivo Deracemization

Cloning was performed to construct three plasmids (i.e., pCDFDuet-ARTA, pCDFDuet-ARTA/TD and pRSFDuet-OATA$_{W58L/R417A}$) using pCDFDuet-1 and pRSFDuet-1 expression plasmids (Novagen) as parental vectors. For construction of pCDFDuet-ARTA, the gene encoding ARTA was amplified from pET28-ARTA, constructed in a previous study,[34] using a forward (5′-GATATACATATGGCATTCAGCGCCGATA-3′) and a reverse primer (5′-CTCGAGGGTACC TCAATACTGAACCGGTGT-3′). The PCR product and the pCDFDuet-1 vector were digested by *Nde*I/*Kpn*I and then ligated using T4 DNA ligase after agarose gel purification. The pCDFDuet-ARTA/TD plasmid was prepared by cloning the *ilvA* gene encoding threonine deaminase into pCDFDuet-ARTA. Gene amplification was performed using a pET21 plasmid harboring *ilvA*, created in a previous study,[35] as a template with a forward (5′-ATAAGGAGATATACCATGGC TGACTCGCAACCC-3′) and a reverse primer (5′-ATTATGCGGCCGCAAGCTTTTAACCCG CCAAAAAGAA-3′). The PCR product was ligated with a linearized pCDFDuet-ARTA, digested with *Nco*I/*Hind*III, using an In-Fusion HD Cloning Kit (Clontech Laboratories). For construction of pRSFDuet-OATA$_{W58L/R417A}$, the *ω-ta* gene encoding OATA$_{W58L/R417A}$ was amplified from pET28-OATA$_{W58L/R417}$, created in this study, using a forward (5′-GATATACATATGACTGCTC AGCCAAAC-3′) and a reverse primer (5′-CTCGAGGGTACCTTACCTGGTGAGGCTTGC-3′). The PCR product and a linearized pRSFDuet-1 vector, both cut by *Nde*I/*Kpn*I, were ligated using

T4 DNA ligase.

In vivo Deracemization Using Engineered E. coli

Deracemization reactions were done at 37 °C and 460 Torr in 50 mM potassium phosphate buffer (pH 7). Typical reaction volume was 1 mL and the reaction mixture was mixed by a magnetic stirrer. For deracemization using glucose as an amino acceptor precursor, *E. coli* BL21(DE3) cells harboring pCDFDuet-ARTA and pRSFDuet-$OATA_{W58L/R417A}$ were used. The reaction conditions were 50 mM *rac*-**1a**, 200 mM **5**, 7.5 - 50 mM glucose and 25.8 mg dcw/mL engineered *E. coli* cells. The reaction was stopped at predetermined reaction times by adding aliquots (typically 10 μL) of reaction mixture into 60 μL of acetonitrile or 127.5 μL of 4.7 % (v/v) $HClO_4$ solution for analyses of hydrophobic or hydrophilic compounds, respectively. After centrifugation (13,000 rpm, 10 min), the supernatant was subjected to HPLC analysis.

For deracemization using L-threonine as an amino acceptor precursor, *E. coli* BL21(DE3) cells harboring pCDFDuet-ARTA/TD and pRSFDuet-$OATA_{W58L/R417A}$ were used. The reaction was performed at 50 mM *rac*-**1a**, 500 mM **5** and 27.5 mM L-threonine using 17.2 mg dcw/mL engineered *E. coli* cells. The procedures for HPLC sampling and analysis were the same as those for the *in vivo* deracemization using glucose.

HPLC Analysis

HPLC analyses were performed using an Alliance system (Waters Co.), a 1260 Infinity II LC System (Agilent Technologies Inc.) or a YL9300 HPLC system (YL Instrument Co., South Korea). Chiral analyses of **1a-d** were carried out using a Crownpak CR(-) or a Crownpak CR-I(-) column (Daicel Co., Japan) under detection by an UV detector tuned at 200 nm. For quantitative chiral

analyses of **1e**, **1f** and **4**, chiral derivatization with 1-fluoro-2,4-dinitrophenyl-5-L-alanine amide (Marfey's reagent) was employed as described elsewhere.[36] The reaction sample was analyzed using a Symmetry C18 column (Waters Co.) at 340 nm. Detailed HPLC analysis conditions were described in Table S4.

Analysis of **2a** was carried out using the Symmetry C18 column with isocratic elution of 60/40 % (v/v) MeOH/water eluent, both containing 0.1 % (v/v) trifluoroacetic acid, at 0.6 mL/min by an UV detector tuned at 254 nm. Retention time of **2a** was 6.5 min.

Key metabolites in the *in vivo* deracemization were analyzed using an Aminex HPX-87H column (Bio-Rad Inc.). Elution was carried out with 5 mM H_2SO_4 at 0.4 mL/min. Organic acids were detected by an UV detector (210 nm). For detection of glucose and ethanol, a RI detector was used under the temperature control at 35 °C. Retention times were 13.3 (glucose), 13.7 (**3**), 19.1 (lactate), 22.7 (acetate) and 30.3 min (ethanol).

RESULTS AND DISCUSSION

Identification of the Competing Reactions

To identify undesirable reactions to be suppressed, we carried out reaction pathway analysis of the competing reactions. To this end, α-methylbenzylamine (**1a**) was chosen as a model amine owing to availability of equilibrium constant (K_{eq}) data.[34] Note that ω- TA harbors pyridoxal 5′-phosphate (PLP) as a prosthetic group.[25] It shuttles between two enzyme forms, i.e. a PLP-form (E-PLP) and a pyridoxamine 5′-phosphate form (E-PMP), to mediate two half reactions consisting of oxidative deamination of an amino donor and reductive amination of an acceptor (Scheme 2). Hence, five half reactions should be considered in the reaction pathway analysis (Table 1). Owing to the

opposite stereoselectivity of the ω-TAs, I^R and III^D are catalyzed by ARTA and so are I^S and III^L by OATA. Note that absolute configurations of D and L-alanine (**4)** are *R* and *S*, respectively. Because **5** is achiral, reaction II is carried out by both ω-TAs.

Combining the two half reactions listed in Table 1, one in a forward and the other in a reverse direction, cancels out the enzyme terms and leads to construction of a whole catalytic cycle. For example, an ARTA reaction between *R*-**1a** and **3** can be represented by adding I^R to the reverse of III^D. We denote the resulting reaction as I^R/III^D. Likewise, an OATA reaction between **5** and acetophenone (**2a**) can be denoted as II/I^S. Consideration of stereoselectivity and reversibility of the ω-TA reactions leads to twelve possible reactions that occur in the reaction mixture (Table 2). Among the twelve reactions, I^R/III^D and II/I^S are the ones constituting the desired deracemization pathway in Scheme 1A.

Thermodynamic Control of the Competing Reactions

Successful deracemization depends on how effectively the unwanted reactions are suppressed while the two desired reaction are unaffected or reinforced. The twelve competing reactions are listed in descending order of equilibrium constants (Table 3). Note that the two reactions in the same row are thermodynamically equivalent because they differ only in chirality. As a first step for the reaction pathway control, we carried out thermodynamic analysis of the twelve reactions. Because reactions I/III, II/III and I/II are exergonic ($\Delta G_{reaction} < 0$), suppression of these reactions is not thermodynamically feasible. In the case of endergonic reactions whose K_{eq} values are < 1, maximum conversions when starting with the same molar concentrations of substrates were calculated to be 20, 11 and 3 % for reactions II/I, III/II and III/I, respectively. Therefore, the intrinsic thermodynamic constraint does not ensure sufficient suppression of II/I and III/II while

the most unfavorable reaction III/I could be regarded negligible.

As a second step, we explored an artificial thermodynamic constraint which could be set up under certain process conditions. We posited that removal of acetone (**6**) under reduced pressure would suppress reactions I/II and III/II where **6** is one of the two substrates. Note that selective removal of **6** is implementable without undesirable coevaporation of **2a**, as demonstrated before,[28, 32] because of a big difference in the boiling point (i.e., 56 vs 202 ^{o}C at 1 atm). Therefore, equilibrium positions of reactions I/III and III/I do not change under the reduced pressure conditions while those of II/III and II/I are completely displaced to the product side. It is notable that the energetically unfavorable II/I^{S}, i.e. one of the two desired reactions, could be driven to completion owing to the equilibrium shift.

Kinetic Control of the Competing Reactions

As aforementioned, the thermodynamic filtering of undesirable reactions would allow suppression of III^{D}/I^{R} and III^{L}/I^{S} by the intrinsic equilibrium and I^{R}/II, I^{S}/II, III^{D}/II and III^{L}/II by the process engineering (Figure 1). However, four reactions (i.e., I^{S}/III^{L}, II/III^{D}, II/III^{L} and II/I^{R}) still remain to be suppressed. This is a challenging task to be tackled by thermodynamic control because the two desired reactions should be allowed to go to completion while their energetic equivalents, i.e. I^{S}/III^{L} and II/I^{R}, are to be suppressed. We reasoned that this might be accomplished by kinetic control based on protein engineering that could provide desirable orthogonality in substrate utilization of the two ω-TAs. For the kinetic control, we paid attention to the half reaction III^{L} because this is a part of the two undesired reactions, i.e. I^{S}/III^{L} and II/III^{L}. We postulated that suppression of these two reactions could be attained if OATA lost its native activity for **3**. To this end, R417A substitution was decided to be introduced because R417 is an active site arginine

responsible for recognition of a carboxylate group of an incoming substrate.[36] We posited that the resulting OATA mutant ($OATA_{R417A}$) would lack the catalytic competence for amination of **3** as well as deamination of L-**4**.

For suppression of the remaining unwanted reactions II/III^D and II/I^R, we noticed that an activity of ARTA for **5** was much lower than that for *R*-**1a** (i.e., 2 % relative activity).[37] Note that the activity of OATA for **5** is 43 % relative to that for *S*-**1a**.[37] However, this does not ensure that II/III^D and II/I^R would occur at negligible reaction rates during the cascade reaction. Hence, we devised additional measures to render II/III^D and II/I^R kinetically insignificant. In the case of II/III^D, we expected that precise control over a feeding amount of **3** would prevent unnecessary reaction progress. Assuming the lack of enzyme activity of $OATA_{R417A}$ for **3**, ARTA would consume most of **3** via either I^R/III^D or II/III^D. Because of the 2 % reactivity of **5** relative to *R*-**1a**,[37] I^R/III^D would proceed 50-fold faster than II/III^D. Therefore, addition of **3** to the reaction mixture slightly over a molar equivalent of *R*-**1a** would render II/III^D terminated upon depletion of *R*-**1a** via I^R/III^D because **3** would not be available any more. In the case of II/I^R, equilibrium is shifted to the product side under reduced pressure and thereby failure to effectively suppress the reaction leads to significant chiral impurity of the resulting *S*-**1a** product. Therefore, the reaction rate of II/I^R should be much lower than that of II/I^S. Based on the previous results,[32] we reasoned that the requisite of II/I^S much faster than II/I^R could be fulfilled by protein engineering of OATA to improve activities for **5** and **2a**. To this end, we decided to introduce an additional mutation to $OATA_{R417A}$, i.e. W58L that was found to elicit remarkable activity improvements for various ketones (e.g., 340-fold increase in k_{cat}/K_M for **2a**) as well as **5** (i.e., 9-fold increase in k_{cat}/K_M) in a previous study.[32]

Protein Engineering of OATA

To implement the proposed kinetic filtering as shown in Figure 1, I^R/III^D should overwhelm the three reactions competing for cosubstrate **3**, i.e. I^S/III^L, II/III^L and II/III^D. Likewise, II/I^S should be much faster than II/I^R to ensure high enantiopurity of the *S*-**1a** product. To verify feasibility of the kinetic control design via protein engineering of OATA, we prepared and purified the $OATA_{W58L/R417A}$ variant (Figure S1). Reaction rates of $OATA_{W58L/R417A}$ for I/III, II/I and II/III were measured and compared with those of ARTA (Table 4). Indeed, the reaction rate of ARTA for I^R/III^D was much higher than that of ARTA for II/III^D as well as those of $OATA_{W58L/R417A}$ for I^S/III^L and II/III^L. Besides, the reaction rate of $OATA_{W58L/R417A}$ for II/I^S was 117-fold higher than that of ARTA for II/I^R. Taken together, $OATA_{W58L/R417A}$ turned out to exhibit desirable kinetic properties to fulfill the kinetic filtering conditions.

In the protein engineering of OATA, we posited that the activity changes, each resulting from R417A and W58L, would not interfere with each other because the two residues belong to different subdomains and are not directly adjacent (Figure S2). Indeed, an activity improvement of $OATA_{W58L/R417A}$ for II/I^S, compared with the parental enzyme, was 600-fold (Table 4) which is even higher than a 165-fold activity increase caused by a single W58L mutation observed in a previous study.[32] In addition, the R417A substitution turned out to abolish an activity of $OATA_{W58L}$ for **3**. Activity of $OATA_{W58L/R417A}$ for I^S/III^L was only 0.16 % compared with that of $OATA_{W58L}$ (Table S5). Owing to the activity loss for **3**, $OATA_{W58L/R417A}$ showed only 0.4 % activity for II/III^L compared with the wild-type enzyme (Table 4). In contrast, the enzyme activity was not affected by R417A when the activity assay was carried out with an amino acceptor, devoid of a carboxyl group, such as propanal (Table S6). It is notable that incorporation of both intended properties into OATA (i.e., reinforcing II/I^S and suppressing I^S/III^L and II/III^L) led to a complete change in the amino acceptor bias from **3** to **2a**. The II/I^S-to-II/III^L reaction rate ratio was

dramatically increased from 4.9×10^{-4} for the parental enzyme to 72 for $OATA_{W58L/R417A}$ (i.e., 1.5×10^5-fold increase), in line with experimental results showing actual partitioning of the amino group of **5** in the presence of both **2a** and **3** (Table S7).

Computational Modeling of the Cascade Reaction

ω-TA is a bisubstrate enzyme following a ping-pong bi-bi mechanism, leading to complicated formulation of enzyme kinetics.[38] Therefore, reaction progresses were obtained under pseudo-second-order approximations of enzyme kinetics. In the mathematical modeling of the deracemization cascade, six reactions among twelve in total were discarded owing to the thermodynamic filtering. The remaining six reactions, i.e. I^R/III^D, I^S/III^L, II/III^D, II/III^L, II/I^R and II/I^S, were considered for the mathematical formulation of deracemization. We assumed that removal of **6** under reduced pressure would be achieved efficiently enough to approximate that concentration of **6** could be negligible throughout the reaction (i.e., $[6]_t \approx 0$). Using Eq. 1, mass balance equations for the five chemical species were derived as follows.

$$\frac{\mathrm{d}[R\text{-}\mathbf{1a}]_t}{\mathrm{dt}} = -k_{I^R/III^D}[R\text{-}\mathbf{1a}]_t[\mathbf{3}]_t + k_{II/I^R}[\mathbf{5}]_t[\mathbf{2a}]_t \quad \text{(Eq. 3)}$$

$$\frac{\mathrm{d}[S\text{-}\mathbf{1a}]_t}{\mathrm{dt}} = -k_{I^S/III^L}[S\text{-}\mathbf{1a}]_t[\mathbf{3}]_t + k_{II/I^S}[\mathbf{5}]_t[\mathbf{2a}]_t \quad \text{(Eq. 4)}$$

$$\frac{\mathrm{d}[\mathbf{3}]_t}{\mathrm{dt}} = -k_{I^R/III^D}[R\text{-}\mathbf{1a}]_t[\mathbf{3}]_t - k_{I^S/III^L}[S\text{-}\mathbf{1a}]_t[\mathbf{3}]_t - k_{II/III^D}[\mathbf{5}]_t[\mathbf{3}]_t - k_{II/III^L}[\mathbf{5}]_t[\mathbf{3}]_t \quad \text{(Eq. 5)}$$

$$\frac{\mathrm{d}[\mathbf{5}]_t}{\mathrm{dt}} = -k_{II/I^R}[\mathbf{5}]_t[\mathbf{2a}]_t - k_{II/I^S}[\mathbf{5}]_t[\mathbf{2a}]_t - k_{II/III^D}[\mathbf{5}]_t[\mathbf{3}]_t - k_{II/III^L}[\mathbf{5}]_t[\mathbf{3}]_t \quad \text{(Eq. 6)}$$

$$\frac{\mathrm{d}[\mathbf{2a}]_t}{\mathrm{dt}} = -k_{II/I^R}[\mathbf{5}]_t[\mathbf{2a}]_t - k_{II/I^S}[\mathbf{5}]_t[\mathbf{2a}]_t + k_{I^R/III^D}[R\text{-}\mathbf{1a}]_t[\mathbf{3}]_t + k_{I^S/III^L}[S\text{-}\mathbf{1a}]_t[\mathbf{3}]_t \quad \text{(Eq. 7)}$$

Computational simulations of the reaction progress were carried out using numerical solutions of the five simultaneous differential equations (Eq. 3 - 7).

To predict whether the reaction pathway control permits intended deracemization of *rac*-**1a** into *S*-**1a**, we carried out computational modeling of the cascade reaction starting with 10 mM *rac*-**1a**, 5.5 mM **3** and 100 mM **5** using four different enzyme pairs (Figure 2). Simulation results predicted that use of wild-type ω-TAs would cause decreases in both enantiomers of **1a** (Figure 2A), consistent with experimental results (Figure S3). Neither of the single-point mutations in OATA was predicted to allow the cascade reaction to result in the intended deracemization, i.e. reaction yield > 90 % (i.e., [*S*-**1a**] > 9 mM) and ee_S > 95 % (Figure 2B and 2C). Simulation results showed that such a desired reaction progress was obtainable only with a ARTA/$OATA_{W58L/R417A}$ pair (Figure 2D). However, the model prediction suggested that *R*-**1a** was not sufficiently consumed to allow ee_S > 99 % seemingly because of a shortage of **3** available for completion of I^R/III^D (Figure S4). Increase in the concentration of **3** no less than 6.5 mM was predicted to allow ee_S > 99 % with reaction yield > 99 % (Figure S5).

In vitro Deracemization

Based on the simulation results, we performed deracemization of 10 mM *rac*-**1a** with 6.5 mM **3** and 100 mM **5** using ARTA/$OATA_{W58L/R417A}$ (both 10 μM) (Figure 3A). Indeed, the reaction progress looked similar to the simulation result shown in Figure 2D. However, accumulation of *S*-**1a** was much slower than expected for such a fast depletion of *R*-**1a**. As a result, reaction yield of *S*-**1a** was only 73 % after 7-h reaction. Another problem was a non-negligible build-up of *R*-**1a** observed after 2 h, resulting in 95.1 % final ee_S. To boost up the slow accumulation of *S*-**1a**, we increased $OATA_{W58L/R417A}$ level to 100 μM. To attain ee_S > 99 %, we opted to reinitiate I^R/III^D at the final stage of deracemization by adding **3** slightly more than the *R*-**1a** impurity (i.e., a "chiral polishing" step). Indeed, the two modifications led to 95 % reaction yield with 99.1 % ee_S at 7 h

(Figure 3B). In this reaction, we also monitored time-dependent changes of **2a** and **3**. After the initial burst owing to I^R/III^D, concentration of **2a** kept going down to 0.04 mM at 6 h. **3** was below a detection limit from 0.5 h on.

To expand the synthetic applicability of the proposed method, we carried out deracemization of five additional amines shown in Scheme 1B (Table 5). It took 4.2 - 8 h to achieve over 90 % reaction yield and 99 % ee_S starting with 10 mM *rac*-**1b-f** (entry 1-5). In the case of **1d** (entry 3), initial concentration of **3** (i.e., 6.5 mM) turned out to be deficient to allow complete consumption of *R*-**1d**. Thus, **3** was added at 2.1 h (1 mM) to remove the *R*-**1d** leftover (0.6 mM), followed by second feeding (0.3 mM) at 3.7 h for chiral polishing (Figure S6). Besides the analytical scale reactions, we carried out preparative scale reaction with 10-fold higher concentration of **1d** (1.49 g) in a 100 mL reaction volume (entry 6). After 21.5 h, reaction yield reached 85 % with > 99 % ee_S. Product isolation led to 1.01 g of *S*-**1d** (79 % recovery yield) of which structural characterization was done by NMR and HRMS (Figure S7).

In vivo Deracemization

Encouraged by the successful implementation of the reaction pathway control, we moved on to construction of a synthetic metabolic pathway enabling the deracemization cascade in a live microbe where **3** is available from a much cheaper precursor by endogenous glycolysis (Figure 4). Toward this end, *Escherichia coli* BL21(DE3) cells were cotransformed with a low and a high copy number plasmid expressing ARTA and $OATA_{W58L/R417A}$ (pCDFDuet-ARTA and pRSFDuet-$OATA_{W58L/R417A}$, respectively; Figure S8), considering that reaction yield would benefit from a high activity of $OATA_{W58L/R417A}$ as observed in Figure 3. The resulting cells exhibited 61 and 55 % activities of ARTA and $OATA_{W58L/R417A}$, respectively, relative to those measured with *E. coli* cells

expressing a single ω-TA (Table S8). The engineered cell harbors a deracemization pathway (Dp) where **3** is supplied from glucose by the Embden–Meyerhof–Parnas (EMP) pathway. Note that the engineered cell should undergo anaerobic metabolism due to the lack of oxygen under the reduced pressure conditions. Therefore, NADH generated from the EMP pathway, i.e. 1 mol per mol of **3**, should be consumed in the fermentative pathway (Fp) to maintain redox balance, mandating conversion of **3** to lactate, ethanol and acetate (Figure S9).

The metabolically engineered cells were incubated with 50 mM *rac*-**1a** in the presence of glucose and **5** (0.25 and 4 molar equivalents, respectively, to *rac*-**1a**). Note that 2 mol of **3** is produced per mol of glucose by the EMP pathway. Therefore, 0.25 molar eq. (i.e., 12.5 mM) is a minimal amount of glucose required for completion of I^R/III^D if **3** is flowed exclusively into Dp. It turned out that 0.25 molar eq. afforded complete removal of 25 mM *R*-**1a** at 18 h with significant accumulation of *S*-**1a**, resulting in 99.5 % ee_S and 65 % reaction yield without a chiral polishing step (Figure 5A). **2a** kept decreasing after 3 h but, unlike Figure 3B, depletion of **2a** was much larger than generation of *S*-**1a**, suggesting that **2a** might be hijacked by an unknown metabolic reaction. In line with this result, we observed that an unknown peak grew bigger with respect to reaction time in the HPLC analysis tuned for **2a** whereas the peak did not appear in the *in vitro* deracemization (Figure S10).

To perform flux analysis of **3**, we measured concentrations of key metabolites at 18 h. Glucose was completely consumed, indicating that 25 mM **3** was generated along with 25 mM NADH by the EMP pathway. A substantial amount of **3** was detected (i.e., 0.1 mM), explaining why the chiral polishing step was not needed to attain > 99 % ee_S. The outcomes of Fp were 4.6 (lactate), 4.8 (ethanol) and 2.7 mM (acetate), indicating that 12.1 mM **3** was partitioned into Fp. Taken together with the secretion amount, maximal flux of **3** into Dp is 12.8 mM that is not in accordance

with the complete removal of 25 mM *R*-**1a**. A possible explanation for this disagreement is that **3** might be recycled from D-**4** via L-**4** by alanine racemase and L-alanine dehydrogenase (Figure S11), which is supported by detection of L-**4** in the reaction mixture where the concentration of L-**4** was 1.7-fold higher than that of D-**4** at 18 h.

To examine how the change in glycolytic flux affects deracemization performance, the feeding amount of glucose was varied from 0.15 to 1 molar eq. Increases in the glucose feeding led to increasing glucose consumption and glucose leftover was observed from 0.5 eq. on (Table S9). Compared with 0.25 eq., increasing glucose feeding caused gradual reduction in the reaction yield although enantiopurity of the resulting *S*-**1a** was further increased (Figure 5B). In line with the pyruvate recycling hypothesis, use of 0.15 eq. glucose (i.e., 7.5 mM) afforded reaction yield as good as that obtained with 0.25 eq. However, complete removal of *R*-**1a** was not achieved and the resulting enantiopurity was only 96.3 % ee_S. This result is seemingly ascribable to a shortage of **3** when starting with 0.15 eq. glucose, consistent with a non-detectable level of **3** in the reaction mixture.

It is notable that lactate formation in the engineered *E. coli* was unusually high compared to that observed in anaerobic cultivation of wild-type cells (i.e., < 0.2 mM) at similar glucose feeding.[39-40] The overflow of **3** to lactate seems to be relevant to NADH overload that caused undesirable generation of toxic products in Fp. In the previous reports, we demonstrated that threonine deaminase (TD) could readily convert L-threonine, a cheap amino acid, to 2-oxobutyrate that is a good amino acceptor for most ω-TAs.[35, 41] Therefore, we posited that Fp could be shut down in the engineered *E. coli* by reinforcing expression of native TD and replacing glucose with L-threonine (Figure S12). To this end, the *ilvA* gene encoding TD of *E. coli* was cloned in pCDFDuet-ARTA and *E. coli* BL21(DE3) was cotransformed with the resulting plasmid (i.e., pCDFDuet-ARTA/TD;

Figure S13) and pRSFDuet-OATA$_{W58L/R417A}$. The resulting engineered cells expressing TD and both ω-TAs were incubated with 50 mM *rac*-**1a**, 27.5 mM L-threonine and 500 mM **5** at 17.2 mg dcw/mL, 37 °C and 460 Torr. After 23.5 h, reaction yield reached 71 % and ee_S was 99.1 %.

CONCLUSION

We have demonstrated deracemization of chiral amines *in vitro* and *in vivo* using reaction pathway control. Engineered orthogonality in the substrate range of enantiocomplementary ω-TAs enabled specific partitioning of common cosubstrates to an intended reaction step. Our strategy illustrates how to cope with unfavorable reaction equilibrium and promiscuous substrate specificity that often remain a challenge in designing a scalable cascade reaction. Besides the deracemization to *S*-amine studied here, deracemization to an antipode enantiomer would be implementable using the same set of substrates if the ω-TA pair fulfills the desired substrate orthogonality. For example, an ARTA mutant engineered for sitagliptin production (ARTA$_{mut}$) is known to display activity improvements for ketones and **5**.[28] So, combination of a *S*-selective ω-TA that lacks activity for **5** and an ARTA$_{mut}$ variant that loses activity for **3** would afford deracemization to *R*-amine. The deracemization cascade was successfully incorporated in *E. coli* where native glycolysis or reinforced deamination of L-threonine was exploited to supply α-keto acid from a cheap precursor. Further engineering of the synthetic microbe is demanded to improve reaction yield, which might involve reinforcement of a crucial bottleneck step (seemingly II/I^S), abolishment of undesirable metabolic interference (hijacking of **2a**) and establishment of metabolic removal of **6**. To the best of our knowledge, this is the first example of an engineered metabolic pathway for deracemization.

ASSOCIATED CONTENT

Supporting Information: The Supporting Information is available free of charge on the ACS Publications website. Thermodynamic calculation of K_{eq} and ΔG. Supporting Tables S1-S9; Supporting Figures S1-S13; HPLC chromatograms.

AUTHOR INFORMATION

Corresponding Author: * E-mail for J.-S.S.: enzymo@yonsei.ac.kr

Notes: The authors declare no competing financial interest.

ACKNOWLEDGMENT

This work was funded by the National Research Foundation of Korea under the Basic Science Research Program (2016R1A2B4008470). Dr. S.-W. Han was financially supported by Initiative for Biological Function & Systems under the BK21 PLUS program of Korean Ministry of Education. We are grateful to the technical work of Saerom Park and Joonhyun Song.

REFERENCES

(1) Sandefur, C. I.; Mincheva, M.; Schnell, S. Network Representations and Methods for the Analysis of Chemical and Biochemical Pathways. *Mol. BioSyst.* **2013**, *9*, 2189-2200.

(2) Feist, A. M.; Herrgård, M. J.; Thiele, I.; Reed, J. L.; Palsson, B. Ø. Reconstruction of Biochemical Networks in Microorganisms. *Nat. Rev. Microbiol.* **2008**, *7*, 129-143.

(3) Rohwer, J. M.; Hofmeyr, J.-H. S. Kinetic and Thermodynamic Aspects of Enzyme Control and Regulation. *J. Phys. Chem. B* **2010**, *114*, 16280-16289.

(4) Chakrabarti, A.; Miskovic, L.; Soh, K. C.; Hatzimanikatis, V. Towards Kinetic Modeling of Genome-Scale Metabolic Networks without Sacrificing Stoichiometric, Thermodynamic and Physiological Constraints. *Biotechnol. J.* **2013**, *8*, 1043-1057.

(5) Bar-Even, A.; Flamholz, A.; Noor, E.; Milo, R. Rethinking Glycolysis: On the Biochemical Logic of Metabolic Pathways. *Nat. Chem. Biol.* **2012**, *8*, 509-517.

(6) Nobeli, I.; Favia, A. D.; Thornton, J. M. Protein Promiscuity and Its Implications for Biotechnology. *Nat. Biotechnol.* **2009**, *27*, 157-167.

(7) France, S. P.; Hepworth, L. J.; Turner, N. J.; Flitsch, S. L. Constructing Biocatalytic Cascades: *In vitro* and *in vivo* Approaches to *de Novo* Multi-Enzyme Pathways. *ACS Catal.* **2017**, *7*, 710-724.

(8) Schrittwieser, J. H.; Velikogne, S.; Hall, M.; Kroutil, W. Artificial Biocatalytic Linear Cascades for Preparation of Organic Molecules. *Chem. Rev.* **2018**, *118*, 270-348.

(9) Sperl, J. M.; Sieber, V. Multienzyme Cascade Reactions—Status and Recent Advances. *ACS Catal.* **2018**, *8*, 2385-2396.

(10) Medema, M. H.; van Raaphorst, R.; Takano, E.; Breitling, R. Computational Tools for the Synthetic Design of Biochemical Pathways. *Nat. Rev. Microbiol.* **2012**, *10*, 191-202.

(11) Tanner, M. E. Understanding Nature's Strategies for Enzyme-Catalyzed Racemization and Epimerization. *Acc. Chem. Res.* **2002**, *35*, 237-246.

(12) Femmer, C.; Bechtold, M.; Roberts, T. M.; Panke, S. Exploiting Racemases. *Appl. Microbiol. Biotechnol.* **2016**, *100*, 7423-7436.

(13) Schrittwieser, J. H.; Groenendaal, B.; Resch, V.; Ghislieri, D.; Wallner, S.; Fischereder, E. M.; Fuchs, E.; Grischek, B.; Sattler, J. H.; MacHeroux, P.; Turner, N. J.; Kroutil, W. Deracemization by Simultaneous Bio-Oxidative Kinetic Resolution and Stereoinversion. *Angew. Chem. Int. Ed.* **2014**, *53*, 3731-3734.

(14) Ghislieri, D.; Turner, N. J. Biocatalytic Approaches to the Synthesis of Enantiomerically Pure Chiral Amines. *Top. Catal.* **2014**, *57*, 284-300.

(15) Carr, R.; Alexeeva, M.; Enright, A.; Eve, T. S. C.; Dawson, M. J.; Turner, N. J. Directed Evolution of an Amine Oxidase Possessing both Broad Substrate Specificity and High Enantioselectivity. *Angew. Chem. Int. Ed.* **2003**, *42*, 4807-4810.

(16) Foulkes, J. M.; Malone, K. J.; Coker, V. S.; Turner, N. J.; Lloyd, J. R. Engineering a Biometallic Whole Cell Catalyst for Enantioselective Deracemization Reactions. *ACS Catal.* **2011**, *1*, 1589-1594.

(17) Köhler, V.; Wilson, Y. M.; Dürrenberger, M.; Ghislieri, D.; Churakova, E.; Quinto, T.; Knörr, L.; Häussinger, D.; Hollmann, F.; Turner, N. J.; Ward, T. R. Synthetic Cascades are Enabled by Combining Biocatalysts with Artificial Metalloenzymes. *Nat. Chem.* **2013**, *5*, 93-99.

(18) Yasukawa, K.; Nakano, S.; Asano, Y. Tailoring D-Amino Acid Oxidase from the Pig Kidney to *R*-Stereoselective Amine Oxidase and Its Use in the Deracemization of α-Methylbenzylamine. *Angew. Chem. Int. Ed.* **2014**, *53*, 4428-4431.

(19) Heath, R. S.; Pontini, M.; Hussain, S.; Turner, N. J. Combined Imine Reductase and Amine Oxidase Catalyzed Deracemization of Nitrogen Heterocycles. *ChemCatChem* **2016**, *8*, 117-120.

(20) Aleku, G. A.; Mangas-Sanchez, J.; Citoler, J.; France, S. P.; Montgomery, S. L.; Heath, R. S.; Thompson, M. P.; Turner, N. J. Kinetic Resolution and Deracemization of Racemic Amines Using a Reductive Aminase. *ChemCatChem* **2018,** 10, 515-519.

(21) Koszelewski, D.; Pressnitz, D.; Clay, D.; Kroutil, W. Deracemization of Mexiletine Biocatalyzed by ω-Transaminases. *Org. Lett.* **2009**, *11*, 4810-4812.

(22) Koszelewski, D.; Clay, D.; Rozzell, D.; Kroutil, W. Deracemisation of α-Chiral Primary Amines by a One-Pot, Two-Step Cascade Reaction Catalysed by ω-Transaminases. *Eur. J. Org. Chem.* **2009**, 2289-2292.

(23) Koszelewski, D.; Müller, N.; Schrittwieser, J. H.; Faber, K.; Kroutil, W. Immobilization of ω-Transaminases by Encapsulation in a Sol-Gel/Celite Matrix. *J. Mol. Catal. B Enzym.* **2010**, *63*, 39-44.

(24) Shin, G.; Mathew, S.; Shon, M.; Kim, B.-G.; Yun, H. One-Pot One-Step Deracemization of Amines Using ω-Transaminases. *Chem. Commun.* **2013**, *49*, 8629-8631.

(25) Malik, M. S.; Park, E. S.; Shin, J. S. Features and Technical Applications of ω-Transaminases. *Appl. Microbiol. Biotechnol.* **2012**, *94*, 1163-1171.

(26) Kelly, S. A.; Pohle, S.; Wharry, S.; Mix, S.; Allen, C. C. R.; Moody, T. S.; Gilmore, B. F. Application of ω-Transaminases in the Pharmaceutical Industry. *Chem. Rev.* **2018**, *118*, 349-367.

(27) Yoon, S.; Patil, M. D.; Sarak, S.; Jeon, H.; Kim, G.-H.; Khobragade, T. P.; Sung, S.; Yun, H., *ChemCatChem* **2019,** 11, 1898-1902.

(28) Savile, C. K.; Janey, J. M.; Mundorff, E. C.; Moore, J. C.; Tam, S.; Jarvis, W. R.; Colbeck, J. C.; Krebber, A.; Fleitz, F. J.; Brands, J.; Devine, P. N.; Huisman, G. W.; Hughes, G. J. Biocatalytic Asymmetric Synthesis of Chiral Amines from Ketones Applied to Sitagliptin Manufacture. *Science* **2010**, *329*, 305-309.

(29) Dawood, A. W. H.; Weiß, M. S.; Schulz, C.; Pavlidis, I. V.; Iding, H.; de Souza, R. O. M. A.; Bornscheuer, U. T. Isopropylamine as Amine Donor in Transaminase-Catalyzed Reactions: Better Acceptance through Reaction and Enzyme Engineering. *ChemCatChem* **2018**, *10*, 3943-3949.

(30) Iwasaki, A.; Yamada, Y.; Kizaki, N.; Ikenaka, Y.; Hasegawa, J. Microbial Synthesis of Chiral Amines by (*R*)-Specific Transamination with *Arthrobacter* sp. KNK168. *Appl. Microbiol. Biotechnol.* **2006**, *69*, 499-505.

(31) Park, E.-S.; Kim, M.; Shin, J.-S. Molecular Determinants for Substrate Selectivity of ω-Transaminases. *Appl. Microbiol. Biotechnol.* **2012**, *93*, 2425-2435.

(32) Han, S. W.; Park, E. S.; Dong, J. Y.; Shin, J. S. Mechanism-Guided Engineering of ω-Transaminase to Accelerate Reductive Amination of Ketones. *Adv. Synth. Catal.* **2015**, *357*, 1732-1740.

(33) Park, E. S.; Shin, J. S. Deracemization of Amino Acids by Coupling Transaminases of Opposite Stereoselectivity. *Adv. Synth. Catal.* **2014**, *356*, 3505-3509.

(34) Park, E.-S.; Malik, M. S.; Dong, J.-Y.; Shin, J.-S. One-Pot Production of Enantiopure Alkylamines and Arylalkylamines of Opposite Chirality Catalyzed by ω-Transaminase. *ChemCatChem* **2013**, *5*, 1734-1738.

(35) Park, E.; Kim, M.; Shin, J.-S. One-Pot Conversion of L-Threonine into L-Homoalanine: Biocatalytic Production of an Unnatural Amino Acid from a Natural One. *Adv. Synth. Catal.* **2010**, *352*, 3391-3398.

(36) Han, S.-W.; Kim, J.; Cho, H.-S.; Shin, J.-S. Active Site Engineering of ω-Transaminase Guided by Docking Orientation Analysis and Virtual Activity Screening. *ACS Catal.* **2017**, *7*, 3752-3762.

(37) Park, E. S.; Dong, J. Y.; Shin, J. S. ω-Transaminase-Catalyzed Asymmetric Synthesis of Unnatural Amino Acids using Isopropylamine as an Amino Donor. *Org. Biomol. Chem.* **2013**, *11*, 6929-6933.

(38) Han, S.-W.; Shin, J.-S. A Facile Method to Determine Intrinsic Kinetic Parameters of ω-Transaminase Displaying Substrate Inhibition. *J. Mol. Catal. B Enzym.* **2016**, *133*, S500-S507.

(39) Trotter, E. W.; Rolfe, M. D.; Hounslow, A. M.; Craven, C. J.; Williamson, M. P.; Sanguinetti, G.; Poole, R. K.; Green, J. Reprogramming of *Escherichia coli* K-12

Metabolism during the Initial Phase of Transition from an Anaerobic to a Micro-Aerobic Environment. *PLoS ONE* **2011**, *6*, e25501.

(40) Murarka, A.; Clomburg, J. M.; Moran, S.; Shanks, J. V.; Gonzalez, R. Metabolic Analysis of Wild-Type *Escherichia coli* and a Pyruvate Dehydrogenase Complex (PDHC)-Deficient Derivative Reveals the Role of PDHC in the Fermentative Metabolism of Glucose. *J. Biol. Chem.* **2010**, *285*, 31548-31558.

(41) Malik, M. S.; Park, E. S.; Shin, J. S. ω-Transaminase-Catalyzed Kinetic Resolution of Chiral Amines using L-Threonine as an Amino Acceptor Precursor. *Green Chem.* **2012**, *14*, 2137-2140.

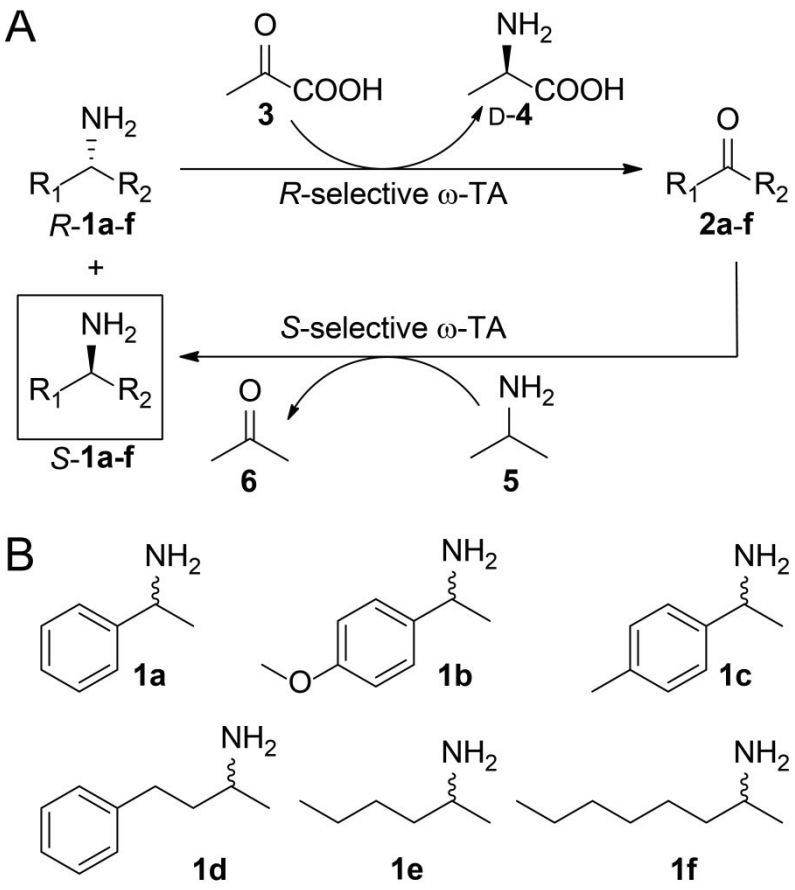

Scheme 1. ω-TA-based deracemization of chiral amines using **3** and **5** as cosubstrates. (A) Conversion of racemic amine into *S*-enantiomer enclosed by a box. (B) Chiral amines used in this study.

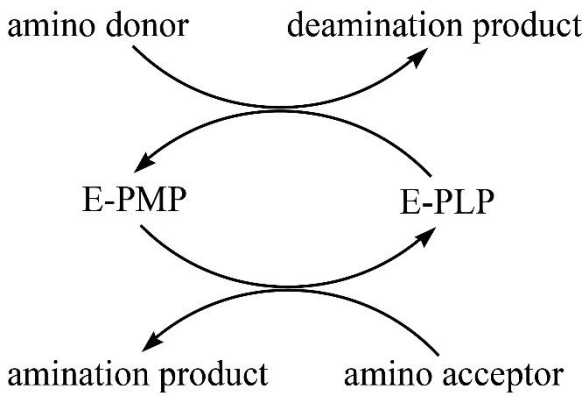

Scheme 2. Whole catalytic cycle of a transaminase reaction consisting of two half reactions.

Table 1. Half reactions occurring among *rac*-**1a**, **3** and **5** in the presence of enantiocomplementary ω-TAs.[a]

Reaction type	Half reaction	Acting enzyme
I^R	*R*-**1a** + E-PLP → **2a** + E-PMP	ARTA
I^S	*S*-**1a** + E-PLP → **2a** + E-PMP	OATA
II	**5** + E-PLP → **6** + E-PMP	both
III^D	D-**4** + E-PLP → **3** + E-PMP	ARTA
III^L	L-**4** + E-PLP → **3** + E-PMP	OATA

[a]Half reactions are shown in the direction of oxidative deamination of an amino donor accompanied by conversion of E-PLP to E-PMP.

Table 2. Chemical equations of the twelve competing reactions occurring among *rac*-**1a**, **3** and **5** in the presence of enantiocomplementary ω-TAs.

Notation	Chemical equation
I^R / III^D	***R*-1a** + **3** → **2a** + D-**4**
I^S / III^L	***S*-1a** + **3** → **2a** + L-**4**
II / III^D	**5** + **3** → **6** + D-**4**
II / III^L	**5** + **3** → **6** + L-**4**
I^R / II	***R*-1a** + **6** → **2a** + **5**
I^S / II	***S*-1a** + **6** → **2a** + **5**
II / I^R	**5** + **2a** → **6** + ***R*-1a**
II / I^S	**5** + **2a** → **6** + ***S*-1a**
III^D / II	D-**4** + **6** → **3** + **5**
III^L / II	L-**4** + **6** → **3** + **5**
III^D / I^R	D-**4** + **2a** → **3** + ***R*-1a**
III^L / I^S	L-**4** + **2a** → **3** + ***S*-1a**

Table 3. Thermodynamic properties of the twelve competing reactions occurring among *rac*-**1a**, **3** and **5** in the presence of ARTA and OATA.[a]

Reaction by ARTA	Reaction by OATA	K_{eq}	$\Delta G_{reaction}$[b] (kJ/mol)
I^R / III^D	I^S / III^L	1130	-18.1
II / III^D	II / III^L	66	-10.8
I^R / II	I^S / II	17	-7.3
II / I^R	II / I^S	5.9×10^{-2}	7.3
III^D / II	III^L / II	1.5×10^{-2}	10.8
III^D / I^R	III^L / I^S	8.8×10^{-4}	18.1

[a]K_{eq} and ΔG values were adopted from a previous study.[34] Detailed calculation procedures are provided in the Supporting Information. [b]The reaction free energies were calculated at 37 °C.

Table 4. Comparison of the reaction rates of ARTA, OATA and $OATA_{W58L/R417A}$ for reactions I/III, II/I and II/III.

Reaction	Specific reaction rate[a] (μM min^{-1} μM-$enzyme^{-1}$)		
	ARTA	OATA	$OATA_{W58L/R417A}$
I / III	110 ± 2	66 ± 3	2.1 ± 0.5
II / I	0.18 ± 0.02	0.035 ± 0.001	21 ± 1
II / III	1.5 ± 0.3	71 ± 9	0.29 ± 0.02

[a]Initial reaction rate per μM enzyme. Reaction conditions were I/III: 5 mM *R* or *S*-**1a** and 5.5 mM **3**, II/I: 100 mM **5** and 5 mM **2a** and II/III:100 mM **5** and 5.5 mM **3**.

Table 5. Deracemization of various chiral amines.[a]

Entry	Amine (mM)	Reaction time (h)	Chiral polishing[b] (h)	Reaction yield[c] (%)	ee_S (%)
1	**1b** (10)	5.5	5	94	99.5
2	**1c** (10)	8	7.5	92	99.0
3	**1d** (10)	4.2	3.7[d]	98	99.1
4	**1e** (10)	5.5	5.2	99	99.5
5	**1f** (10)	8	7.2	90	99.2
6	**1d** (100)[e]	21.5	20[f]	85	99.1

[a]Reaction conditions except entry 6: 10 mM racemic amine, 6.5 mM **3**, 100 mM **5**, 10 μM ARTA, 100 μM $OATA_{W58L/R417A}$ and 15 % v/v DMSO in 50 mM phosphate buffer (pH 7) at 37 °C and 460 Torr. Total reaction volume was 1 mL. [b]It represents the feeding time of **3** at the final concentration of 0.5 mM except entry 3. [c]Calculated by $[S\text{-amine}]_{final}/[rac\text{-amine}]_{initial}$. [d]Besides the chiral polishing, **3** was additionally fed at 2.1 h. [e]Reaction conditions: 100 mM *rac*-**1d**, 80 mM **3**, 200 mM **5**, 10 μM ARTA, 200 μM $OATA_{W58L/R417A}$ and 15 % v/v DMSO in 50 mM Tris buffer (pH 7) at 37 °C and 460 Torr. [f]Final concentration of **3** for the chiral polishing was 1.5 mM.

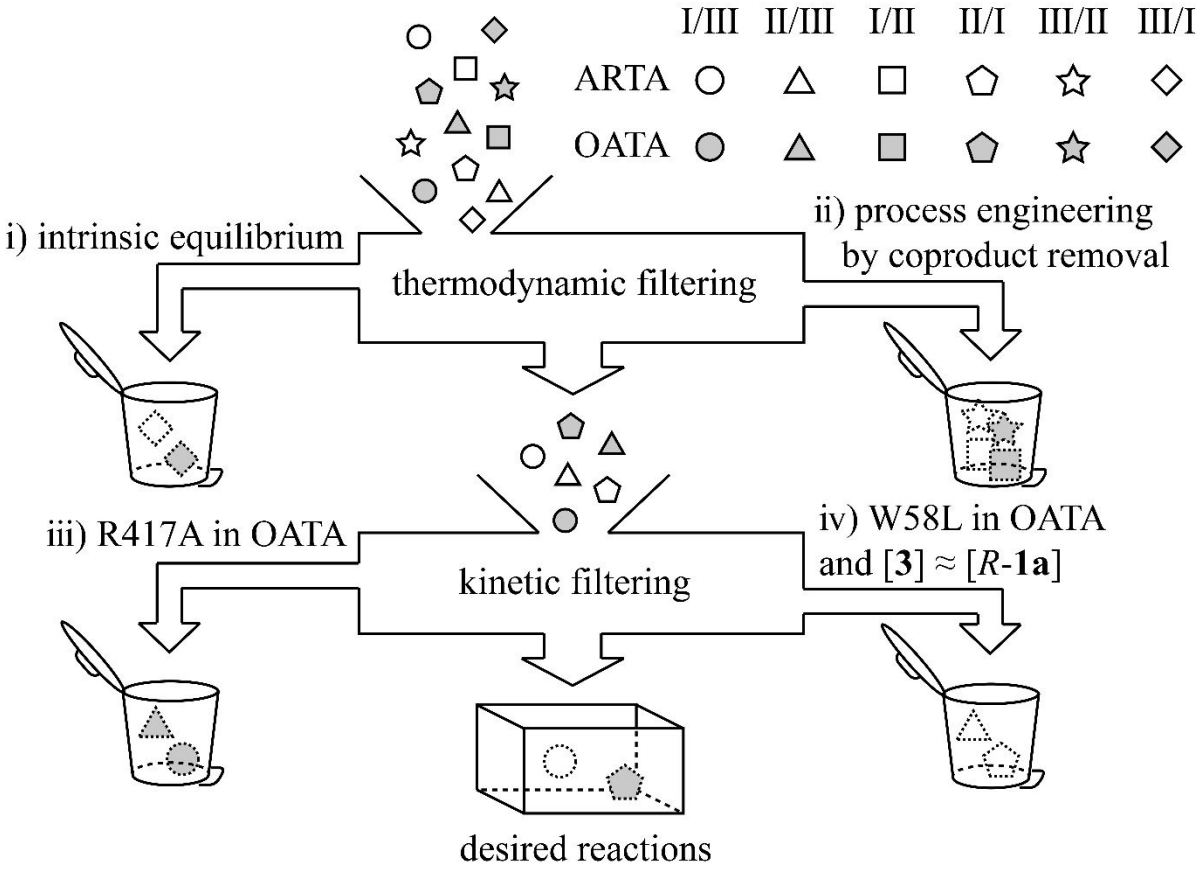

Figure 1. Thermodynamic and kinetic filtering of 10 undesirable reactions among 12 competing ones.

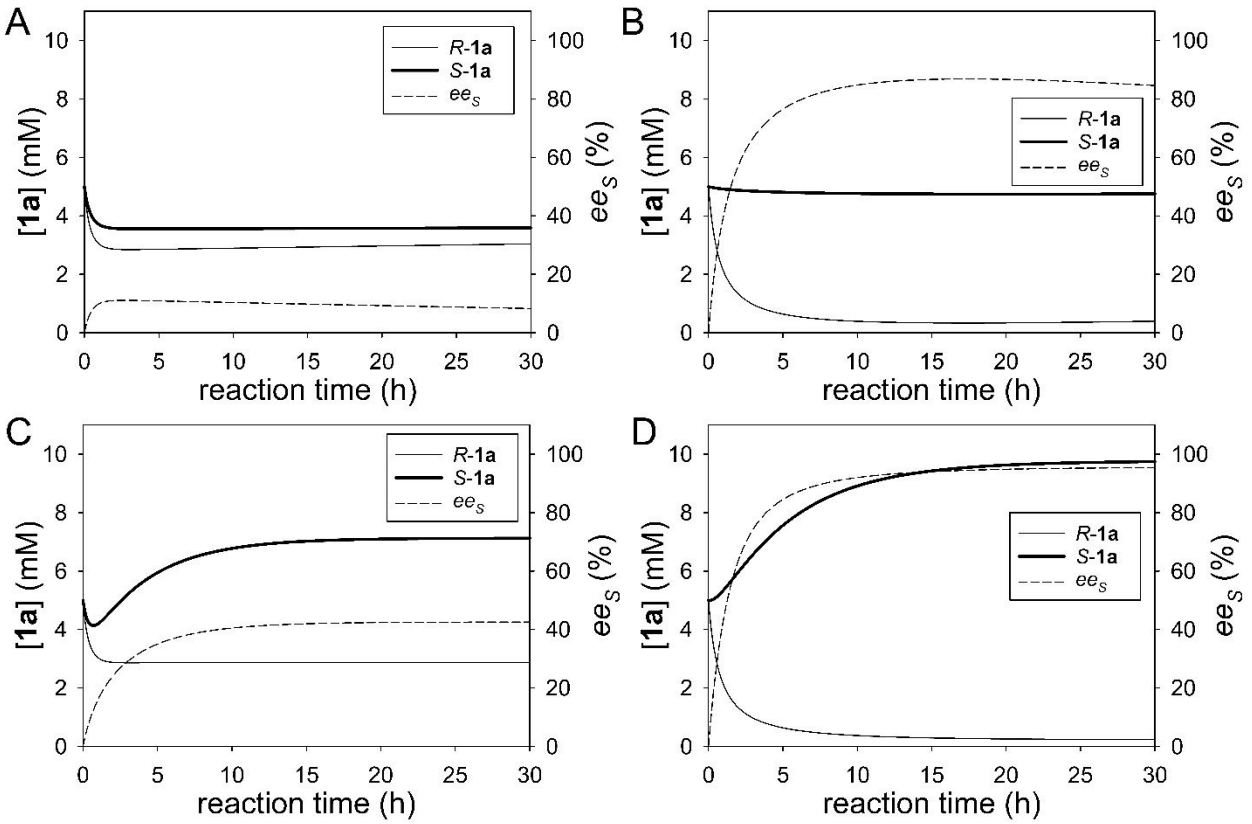

Figure 2. Numerical simulations of the cascade reactions using different enzyme pairs. (A) ARTA/OATA, (B) ARTA/OATA$_{R417A}$, (C) ARTA/OATA$_{W58L}$ and (D) ARTA/OATA$_{W58L/R417A}$. Enzyme concentrations used for the simulations were 1 μM for both ω-TAs.

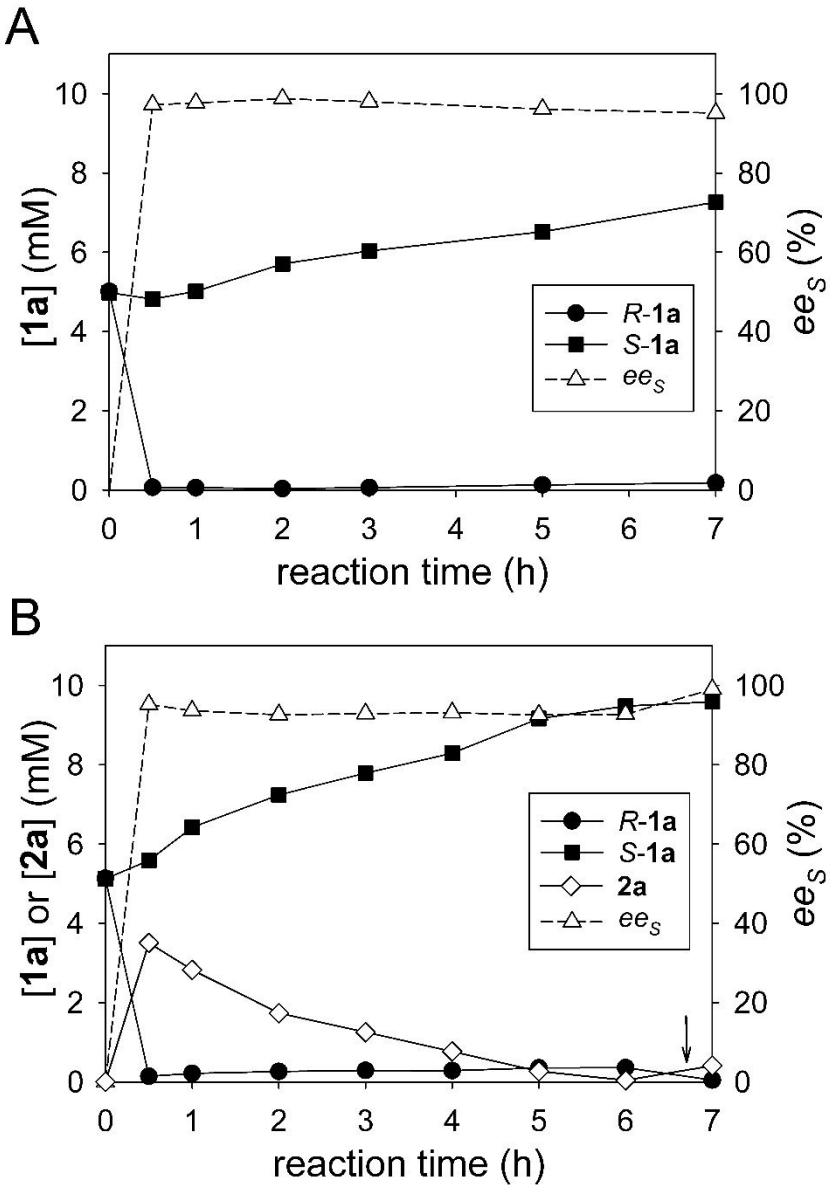

Figure 3. *In vitro* deracemization of *rac*-**1a** with ARTA/OATA$_{W58L/R417A}$. Reaction conditions were 10 mM *rac*-**1a**, 6.5 mM **3**, 100 mM **5** and 50 mM phosphate buffer (pH 7) in a 1 mL reaction mixture at 37 °C and 460 Torr. **(**A) Both ω-TAs were 10 μM. (B) ARTA and OATA$_{W58L/R417A}$ were 10 and 100 μM, respectively. Reaction mixture contained 15 % v/v DMSO. Arrow represents the additional feeding of **3** at 6.7 h (final concentration = 0.5 mM).

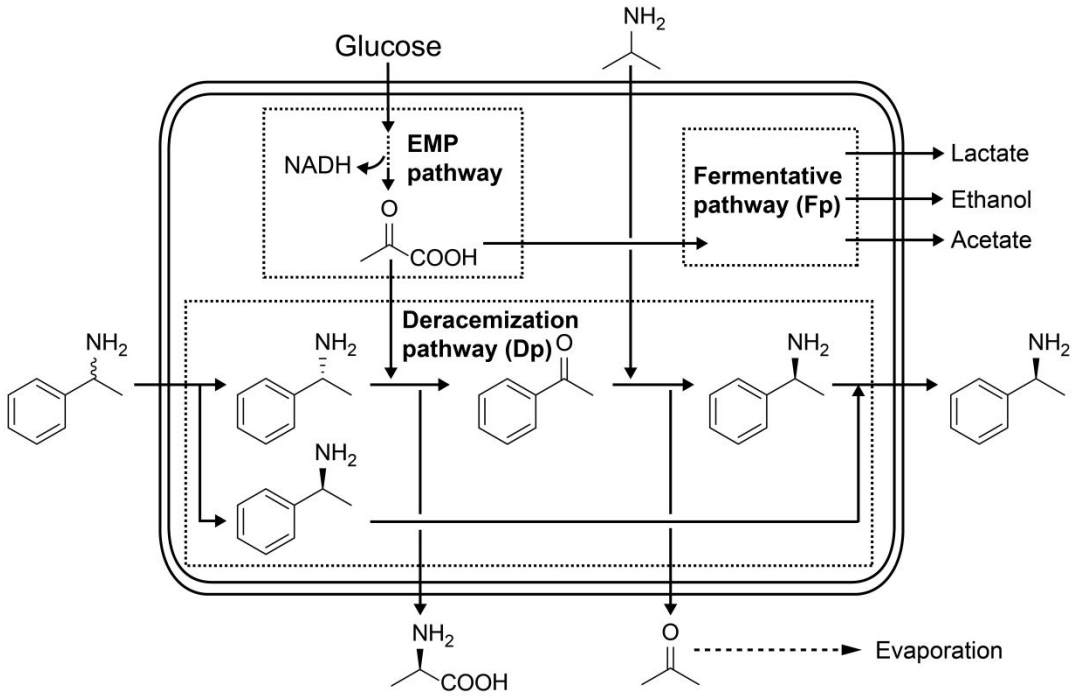

Figure 4. A synthetic metabolic pathway capable of deracemization of chiral amines. *Rac*-**1a** is converted to *S*-**1a** by the engineered *E. coli* in the presence of glucose and **5** under reduced pressure.

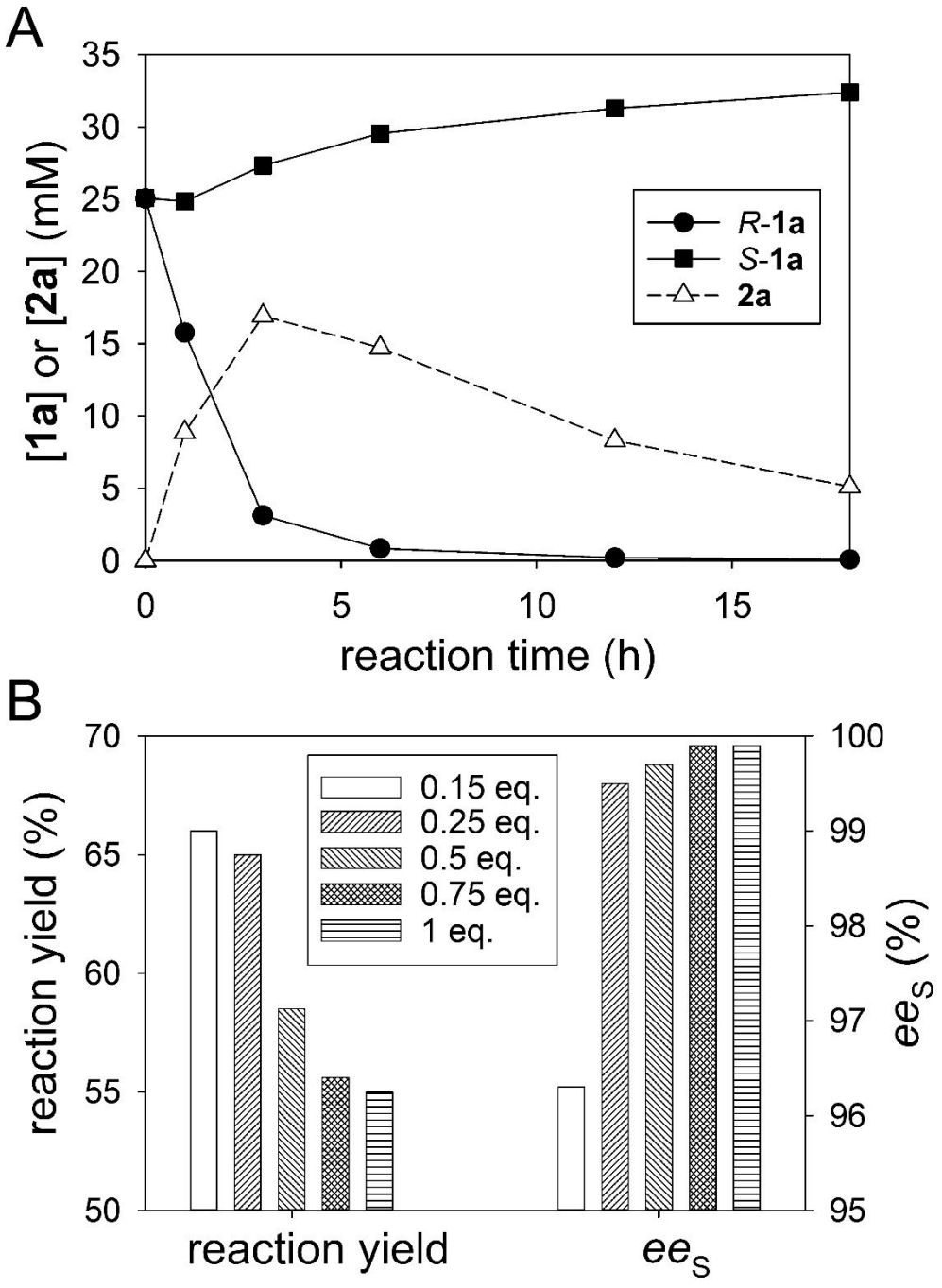

Figure 5. *In vivo* deracemization using glucose as an amino acceptor precursor. (A) Reaction profile for deracemization with 0.25 eq. of glucose. (B) Effect of the glucose feeding amount on reaction yield and ee_S after 18-h reaction. Reaction conditions: 50 mM *rac*-**1a**, 7.5 - 50 mM glucose, 200 mM **5** and the engineered *E. coli* cells expressing ARTA and OATAW58L/R417A (25.8 mg dcw/mL) at 37 °C and 460 Torr.

TOC graphic

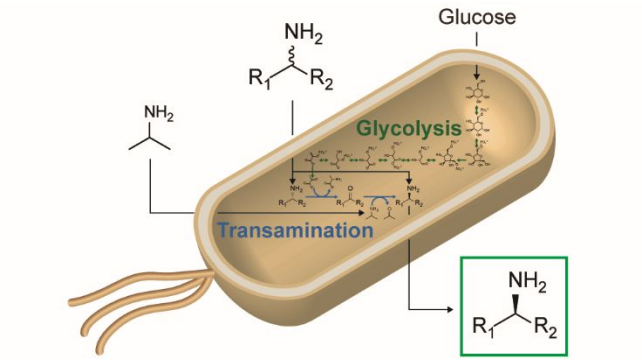

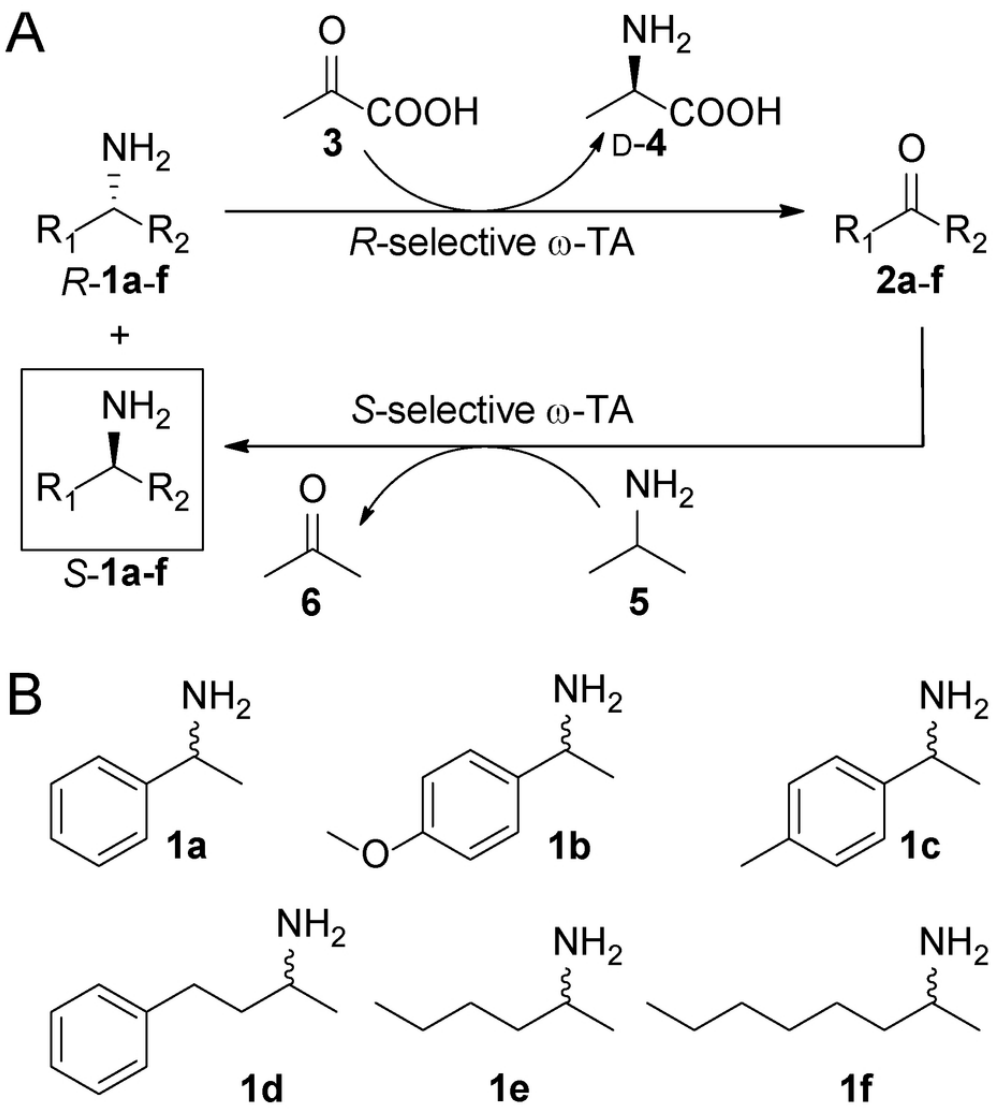

Scheme 1

78x88mm (300 x 300 DPI)

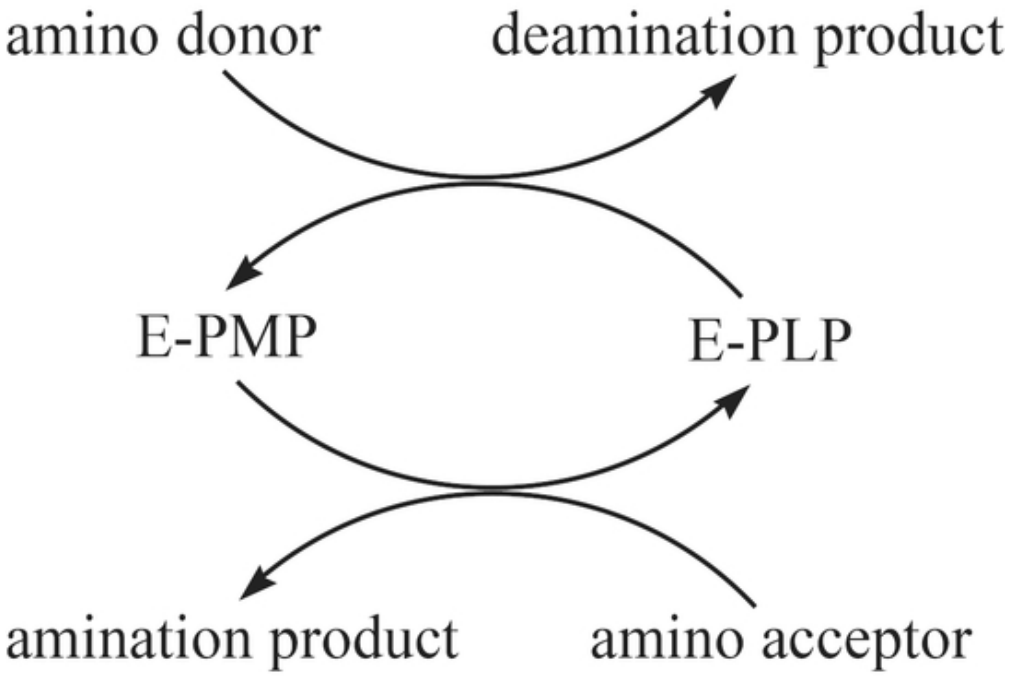

Scheme 2

45x30mm (300 x 300 DPI)

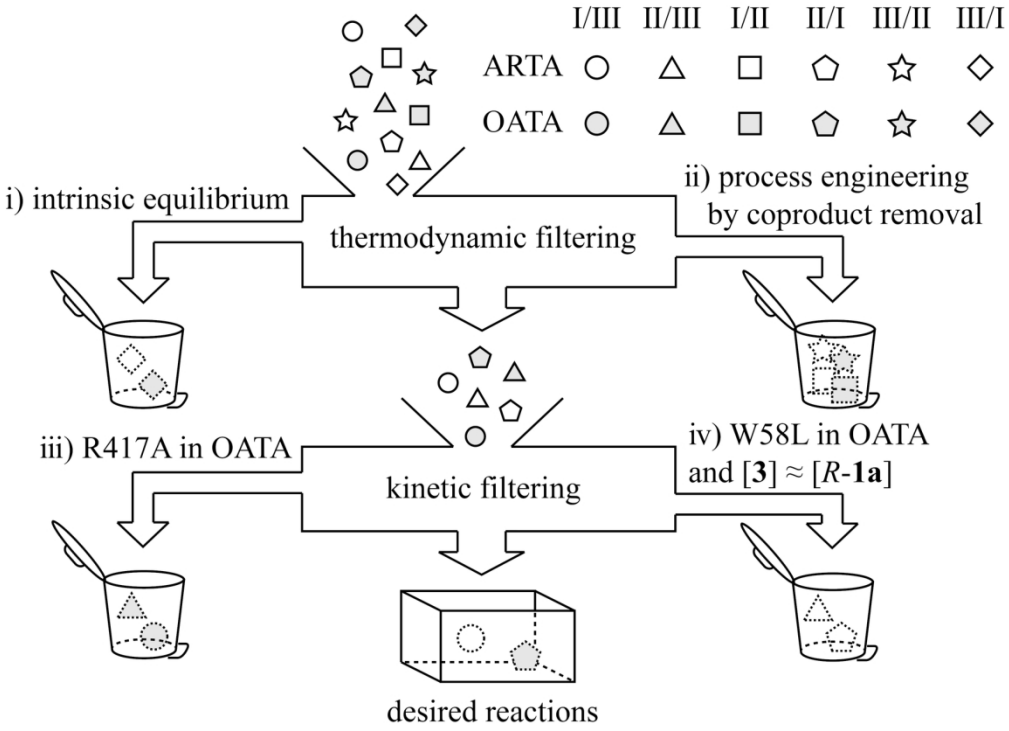

Fig. 1

157x114mm (300 x 300 DPI)

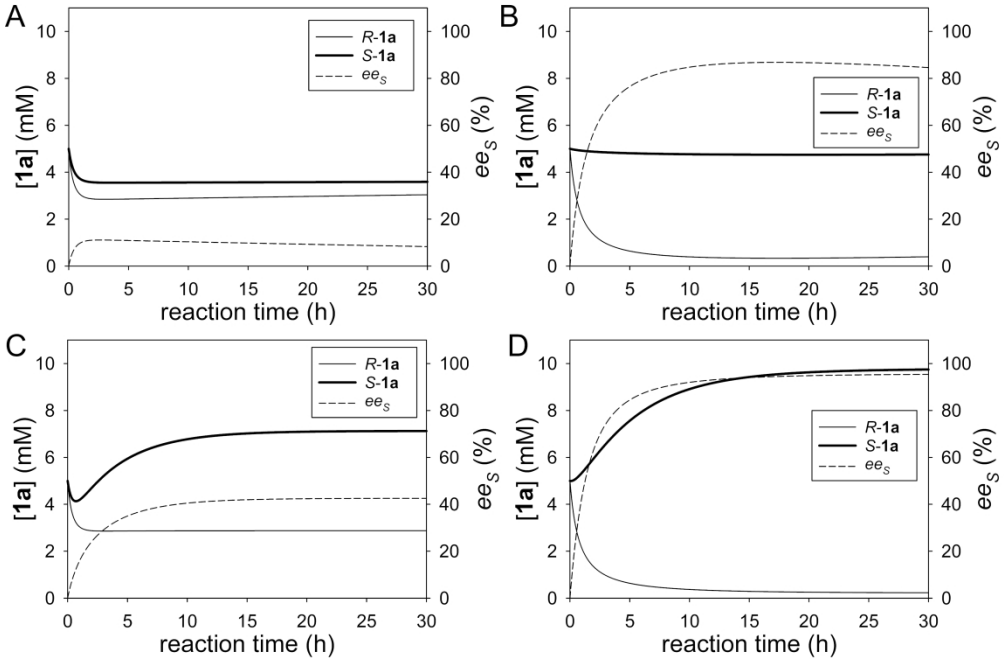

Fig. 2

348x239mm (300 x 300 DPI)

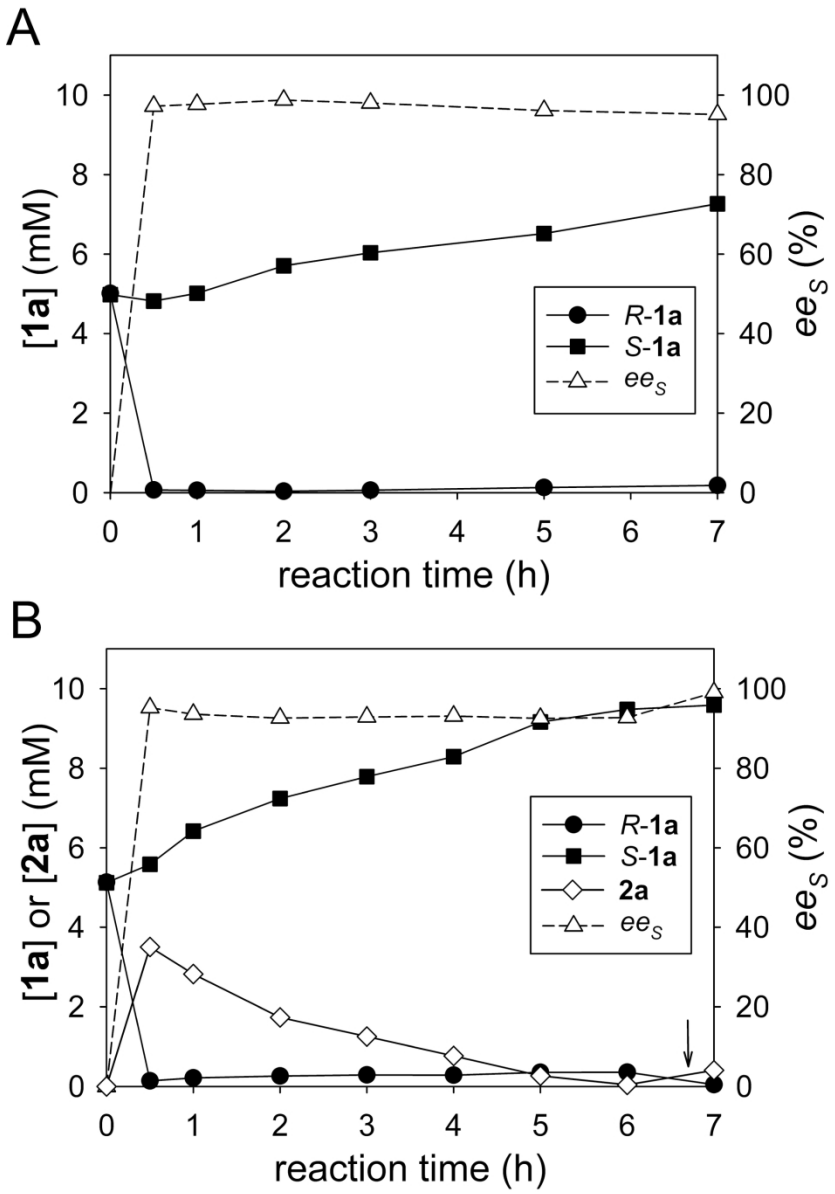

Fig. 3

171x247mm (300 x 300 DPI)

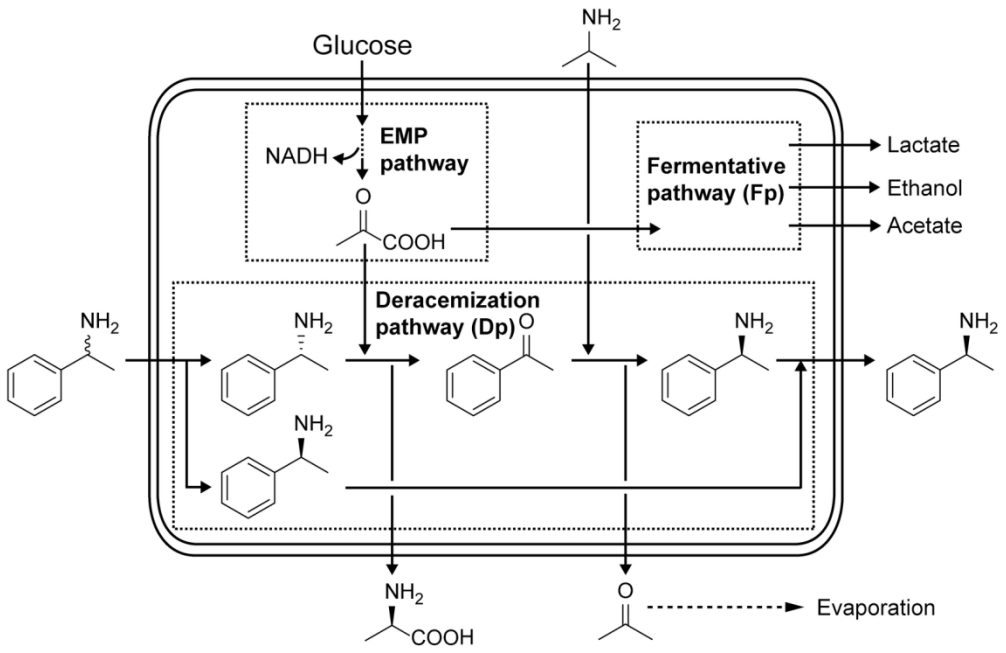

Figure 4

141x91mm (300 x 300 DPI)

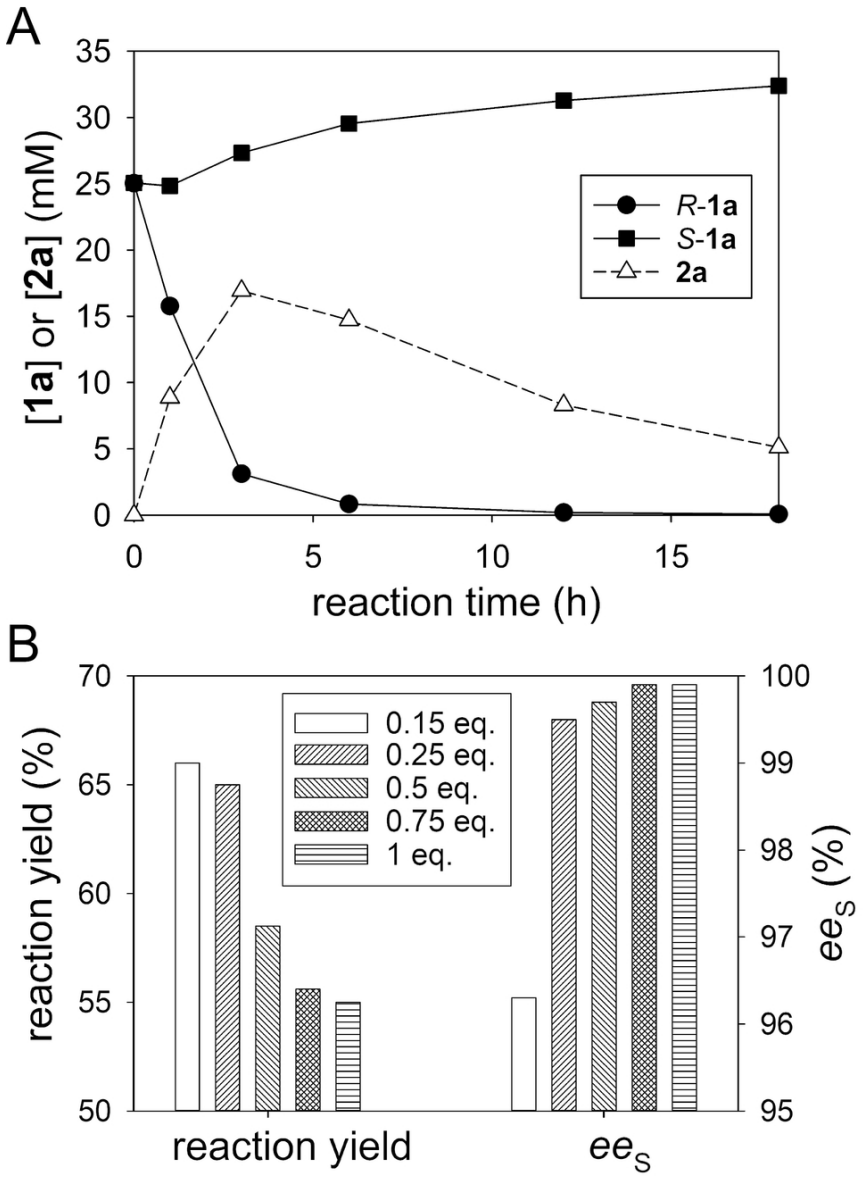

Fig. 5

81x113mm (300 x 300 DPI)

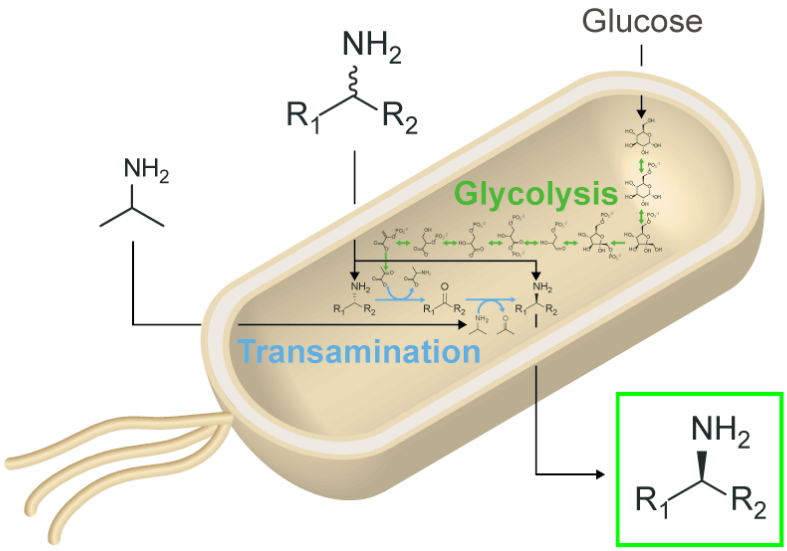

Table of contents graphic